Journal of Inorganic and General Chemistry
ZAAC
Zeitschrift für anorganische und allgemeine Chemie
www.zaac.wiley-vch.de
RESEARCH ARTICLE
Check for updates
DOI: 10.1002/zaac.202300087

Special Collection

Lithium-Filled Skutterudites by Intercalation at Ambient-Temperature

Jesús Prado-Gonjal,[a, d] Paz Vaqueiro,[a] Radoslaw M. Kowalczyk,[b] Ronald I. Smith,[c] and Anthony V. Powell*[a]

Dedicated to Professor Antoine Maignan on the occasion of his 60th birthday

The incorporation of lithium as a filler species in $Co_{1-2x}Fe_xNi_xSb_3$ skutterudites was accomplished by intercalation at 60 °C, using *n*-BuLi as a reducing agent. Solid state ^{7}Li NMR and ICP-MS analysis confirm the presence of lithium in the product phases and provide an estimate of the lithium content. The maximum uptake of lithium increases as cobalt is progressively substituted by an equimolar mixture of iron and nickel. Difference Fourier maps, calculated during Rietveld structure refinement using powder neutron diffraction data, locate the lithium cations at the 2*a* (0,0,0) sites within the cavities of the skutterudite framework. The intercalation of lithium results in reductions in thermal conductivity of up to 47 %, indicative of phonon glass electron crystal (PGEC) type behaviour. Charge transfer from lithium to the framework that accompanies intercalation results in a substantial decrease in electrical resistivity in lithiated phases and a more metal-like temperature dependence. The increased carrier concentration also decreases the Seebeck coefficient, with the consequence that modest increases in the figure of merit occur, despite the reduced thermal conductivity.

Introduction

Thermoelectric devices offer opportunities to convert otherwise waste heat into useful electrical energy in diverse application areas that span a wide range of temperatures.[1] The efficiency of a thermoelectric (TE) device is governed by the properties of the constituent *n*- and *p*-type semiconductors of which it is comprised. Materials performance may be expressed in terms of a dimensionless figure of merit; $ZT = S^2\sigma T/\kappa$. High performance requires a high electrical conductivity (σ), characteristic of a metal, to be coupled with a high Seebeck coefficient (S) and low thermal conductivity (κ); properties that are more usually associated with non-metallic systems. Since there are two contributions to thermal conductivity, arising from electronic (κ_e) and lattice (κ_L) components, a common strategy for improving TE performance is to target a reduction in κ_L, without impairing the electrical-transport properties.[2,3,4,5,6]

An approach that has been used to reduce the lattice thermal conductivity exploits what is termed phonon glass electron crystal (PGEC) behaviour,[7,8] in which weakly-bound filler species are introduced into the cavities of a framework structure. The filler species exhibit localised vibrational modes, termed "rattling" vibrations, that serve to scatter heat-carrying phonons.[9,10] A particularly successful implementation of the PGEC concept is provided by skutterudite materials.[11,12,13,14,15]

The skutterudite structure, of general formula MX_3, consists of a framework of vertex-linked MX_6 octahedra (Figure 1a). The unit cell consists of eight transition-metal cubelets, with planar four-membered X_4 rings located at the centre of six of them (Figure 1b). Filler species, *A*, may be inserted into the remaining empty transition-metal cubelets, yielding a limiting stoichiometry of AM_4X_{12}.[11,16,17,18] Partial occupancy of these interstitial sites within the cavities of the skutterudite framework can lead to substantial reductions in thermal conductivity.[19,20,21] Scattering of heat-carrying phonons is maximised for those phonons with frequencies close to the resonance frequency (ω_0) of the filler (rattler).[22,23] This has led to exploration of skutterudites containing multiple filler species[24,25,26] in an effort to increase the range of the phonon spectrum over which scattering may occur.

In this work, we have sought to extend the typical range of fillers from the commonly used rare-earth ($\omega_0 \approx 70$ cm^{-1}) and alkaline-earth metals ($\omega_0 \approx 90$ cm^{-1}) to alkali-metals ($\omega_0 \approx 150$ cm^{-1}).[27,28,29] Lithiation of skutterudites is not feasible

[a] J. Prado-Gonjal, P. Vaqueiro, A. V. Powell
Department of Chemistry, University of Reading, RG6 6DX, Reading, UK
E-mail: a.v.powell@reading.ac.uk
[b] R. M. Kowalczyk
Chemical Analysis Facility, University of Reading, RG6 6DX, Reading, UK
[c] R. I. Smith
ISIS Facility, Rutherford Appleton Laboratory, Harwell Campus, Didcot OX11 0QX, UK
[d] J. Prado-Gonjal
Present address: Departamento de Química Inorgánica, Universidad Complutense de Madrid, E-28040, Madrid, Spain

Supporting information for this article is available on the WWW under https://doi.org/10.1002/zaac.202300087

This article is part of a Special Collection dedicated to Professor Antoine Maignan on the occasion of his 60th birthday. Please see our homepage for more articles in the collection.

Journal of Inorganic and General Chemistry
ZAAC
Zeitschrift für anorganische und allgemeine Chemie

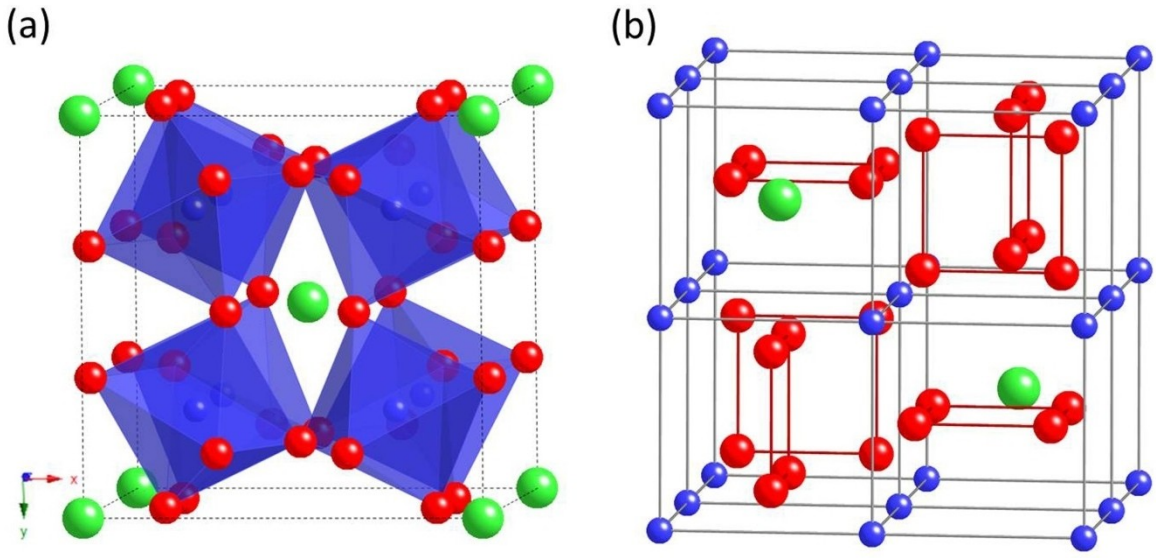

Figure 1. (a) Polyhedral representation of the MX_3 skutterudite structure. (b) Ball and stick representation of the MX_3 structure, showing the planar rectangular four-membered X_4 rings. M (Fe, Co, Ni) in blue, X (Sb) in red and filler species in green.

using conventional high-temperature methods, although it has been shown that Li_xCoSb_3 can be synthesized using high pressure.[28,30] However, investigations of $CoSb_3$-based skutterudites as potential battery cathodes[31,32,33] suggest that lithium may be inserted into the skutterudite cavities by intercalation processes. For this reason, we have exploited ambient-temperature intercalation reactions to introduce lithium cations into the cavities of the skutterudite framework. In this way we have sought to introduce a rattling species with a higher resonance frequency to promote scattering of higher frequency phonons. This approach has been combined with chemical substitution in $CoSb_3$ to produce frameworks of general formula $Co_{1-2x}Fe_xNi_xSb_3$ to provide an additional mechanism for reducing thermal conductivity. In addition to the rattling within the skutterudite cavities, incorporation of lithium results in the transfer of an electron to the skutterudite framework, leading to an increase in carrier concentration that results in significant changes to the electrical-transport properties. To the best of our knowledge, this work represents the first example of the incorporation of lithium as a filler species in skutterudites using an ambient-temperature intercalation reaction.

Experimental

The $Co_{1-2x}Fe_xNi_xSb_3$ ($0 \leq x \leq 0.5$) frameworks were synthesized by grinding stoichiometric amounts of the constituent elements: Co (Alfa Aesar, 99.8%, powder), Fe (Alfa Aesar, 99.9%, powder), Ni (Aldrich, 99.99%, powder) and Sb (Alfa Aesar, 99.5%, powder) using an agate pestle and mortar in an argon-filled glovebox. The reagents were loaded into fused silica tubes which were evacuated ($< 10^{-4}$ Torr) prior to sealing. The mixtures were heated at 923 K for 72 h, using a heating and cooling rate of 1 K min^{-1}

In a typical intercalation reaction, a suspension of *ca.* 3 g of $Co_{1-2x}Fe_xNi_xSb_3$ in 50 mL of anhydrous hexane (Aldrich, 99%) was added to a 2-necked flask attached to a Schlenk nitrogen-vacuum line, and purged with nitrogen. A 10% excess of *n*-BuLi (2.5 M solution in hexane, Aldrich) was added dropwise to the suspension *via* a syringe, over a 3 min period, through a PTFE/silicone septum. The mixture was heated at 60 °C using a hotplate whilst stirring for 24 h. The product was washed under nitrogen, with ethanol, before drying under vacuum. The product was then heated at 80 °C for 3 h in order to remove any organic residue.

Powder X-ray diffraction data for the initially-prepared skutterudite powders, powder products of lithiation and consolidated pellets were collected on a Bruker D8 Advance diffractometer operating with Cu-$K_{\alpha 1}$ radiation ($\lambda = 1.5405$ Å). Data were collected over the angular range $10 \leq 2\theta/° \leq 120$, at steps of $2\theta = 0.0145°$ in detector position.

Solid state ^{7}Li nuclear magnetic resonance spectra were recorded on a Bruker 500 MHz Avance III spectrometer at a Larmor frequency of 194.37 MHz (11.75 T) for ^{7}Li. Single pulse static spectra were recorded using a standard bore 4 mm MAS probe. The 90° pulse length was 12 μs (at the power level of 15 W) and the relaxation delay time was 800 s for the LiCl reference and 10s for all other experiments. Between 256 and 2048 signal transients were accumulated and averaged into a single spectrum. All spectra were recorded without rotation (static) because of their high density. All spectra were referenced to an external LiCl signal at 0 ppm. Inductively Coupled Plasma Mass Spectrometry (ICP-MS was carried out using an Agilent 7700 instrument. Samples for analysis were prepared by digesting *ca.* 50 mg of finely ground powder in aqua regia with the aid of microwave irradiation

Time of flight powder neutron scattering data[34] were collected on the Polaris diffractometer at the ISIS facility, Rutherford Appleton Laboratory.[35] Data were collected at room temperature from *ca.* 3 g of powder contained in a cylindrical thin-walled 6 mm diameter vanadium can. For each sample, data were collected over a period of *ca.* 5 h (700 μA h), providing high-quality data sufficient to generate Fourier maps. Rietveld analysis was carried out using the GSAS program suite[36] in a multi-histogram refinement, incorporating data from the backscattering ($135 < 2\theta/° < 167$) and 90° ($75 < 2\theta/° < 112$) detector banks. 3D and 2D Fourier maps were

calculated in GSAS following refinement of the framework structure only, excluding the positional coordinates of lithium, using VESTA software to provide graphical representations.[37]

Pellets for electrical and thermal transport property measurements were prepared by hot pressing for 30 min at 873 K in a graphite die, under a pressure of 90 MPa in a nitrogen atmosphere. Densities of the hot-pressed pellets of the unfilled skutterudites, determined by the Archimedes method using an AE Adam PW 184 balance, are 98–99% of crystallographic values. Densities of the lithiated materials are slightly lower (90–95% of the crystallographic density) and the pellets were found to be more brittle than those of the unfilled skutterudites. Thermal diffusivity (α) measurements were performed on hot-pressed pellets of $Li_yCo_{1-2x}Fe_xNi_xSb_3$ ($0.0 \leq y \leq 0.29$; $0 \leq x \leq 0.5$) using a Netzsch LFA 447 NanoFlash instrument over a temperature range $300 \leq T/K \leq 573$, in 25 K steps. The thermal conductivity (κ) was calculated using $\kappa = \alpha C_p d$, where C_p is the heat capacity and d is the sample density. In order to maximise the heat absorption, a graphite coating was applied to the surface of the pellet. Pyroceram™ 9606 was used as a reference to determine the heat capacity of the samples. Cowan's model[38] with a pulse correction was applied to calculate α. The lattice (κ_L) contribution of the thermal conductivity was estimated using the electrical conductivity data in conjunction with the Wiedemann–Franz law ($\kappa_e = L\sigma T$), with a Lorenz constant (L) of 2.45×10^{-8} W Ω K^{-2}.

The temperature dependence of the electrical conductivity and Seebeck coefficient was measured simultaneously over the temperature range of $300 \leq T/K \leq 573$, using a Linseis LSR-3 instrument, with samples contained under a partial pressure of He. A 100 mA current was passed through the sample for the electrical conductivity measurements.

Results and discussion

Powder X-ray diffraction data for all materials of general formula $Li_yCo_{1-2x}Fe_xNi_xSb_3$ are indexable on the basis of a body-centered cubic unit cell ($a \approx 9$ Å), consistent with the retention of the skutterudite structure on intercalation. With the exception of a reflection assignable to graphite arising from the die, powder X-ray diffraction data of consolidated pellets exhibit no discernible change as a result of hot pressing (Figure S1). The graphite was removed by polishing with a fine-grade abrasive paper prior to measurement of transport properties. The chemical composition of the synthesized materials was determined by ICP-MS. Within experimental error, transition-metal and antimony contents are similar to those of the stoichiometric composition of the sample (ICP-MS values are summarized in the Supplementary Information). The content of Li for the different nominal compositions, as determined by ICP-MS, is shown in Table 1.

The maximum extent of lithium incorporation is lower than that achieved in previous studies, under conditions of high pressure and temperature ($y \approx 0.4$).[30] For the skutterudites with the highest cobalt contents ($x = 0$, 0.125), the amount of *n*-BuLi used in the reaction has little effect on the degree of lithium incorporation, suggesting a limiting lithium uptake of $y \approx 0.15$ at these framework compositions. This relatively low value is consistent with the rapid drop in potential observed during electrochemical discharge of a cell containing a $CoSb_3$ cathode,[31] to a value (0.8 V *vs* Li^+/Li) that lies below the redox potential of *n*-BuLi ($E \approx 1.0$ V),[39] at which point *n*-BuLi is insufficiently strong a reducing agent to continue to effect further reduction of the partially-reduced framework. As cobalt is replaced by an equimolar mixture of iron and nickel, reduction with *n*-BuLi leads to higher levels of lithium incorporation, suggesting that the framework becomes more reducible as what is formally Co^{3+} is progressively replaced by an equimolar mixture of Fe^{2+}/Ni^{4+}.[40] Moreover, in the mixed-metal materials, differences in lithium uptake as the amount of *n*-BuLi used in the initial reaction become more evident, consistent with a wider potential window and hence higher limiting value of lithium uptake when $x > 0.0$.

Table 1. Lithium contents in $Li_yCo_{1-2x}Fe_xNi_xSb_3$ determined by ICP-MS.

Nominal Composition	y
$Li_{0.25}CoSb_3$	0.15
$Li_{0.1}CoSb_3$	0.13
$Li_{0.25}Co_{0.75}Fe_{0.125}Ni_{0.125}Sb_3$	0.12
$Li_{0.1}Co_{0.75}Fe_{0.125}Ni_{0.125}Sb_3$	0.09
$Li_{0.25}Co_{0.5}Fe_{0.25}Ni_{0.25}Sb_3$	0.21
$Li_{0.1}Co_{0.5}Fe_{0.25}Ni_{0.25}Sb_3$	0.10
$Li_{0.25}Co_{0.25}Fe_{0.375}Ni_{0.375}Sb_3$	0.19
$Li_{0.1}Co_{0.25}Fe_{0.375}Ni_{0.375}Sb_3$	0.09
$Li_{0.25}Fe_{0.5}Ni_{0.5}Sb_3$	0.29
$Li_{0.1}Fe_{0.5}Ni_{0.5}Sb_3$	0.10

^{7}Li solid-state NMR data confirm the presence of lithium in the intercalated materials. Data for the LiCl reference together with those of Li_yCoSb_3, $Li_yCo_{0.5}Fe_{0.25}Ni_{0.25}Sb_3$ and $Li_yFe_{0.5}Ni_{0.5}Sb_3$ ($y = 0.1$ and 0.25) are presented in Figure 2 (the remaining ^{7}Li NMR spectra are provided in Figure S2). In all ^{7}Li spectra a broad single resonance is centred at *ca.* 0 ppm. This differs from ^{7}Li NMR spectra obtained after electrochemical insertion of lithium, where at high levels of discharge (large y), signals at −0.5 ppm and −0.1 ppm, assigned to ionic forms of lithium (Li_2CO_3 and $ROCO_2Li$ species) are observed.[33] The recorded spectra show significant line broadening compared to the reference signal, which is likely to be due to the presence of paramagnetic ions which influence the nuclear spin relaxation.[41,42] Comparison of the ratio of intensities (peak areas) of the peak in the ^{7}Li NMR spectra ($I_{0.25}/I_{0.1}$) for materials with nominal lithium contents of $y = 0.25$ and $y = 0.1$ reveals a reasonable correlation with the ratio of lithium contents determined experimentally by ICP-MS (Table 2) for skutterudites with a low level of framework substitution ($x \leq 0.25$). The divergence of the ratio, $I_{0.25}/I_{0.1}$, from that determined by ICP-MS, at higher iron and nickel contents may reflect the impact of paramagnetic species in broadening the NMR signal, making intensity measurements less reliable.

Although powder X-ray diffraction data are sufficient to confirm retention of the skutterudite structure, they do not provide information on the location of lithium cations, owing to the low X-ray scattering power of lithium, compared to the strong scatterers antimony and the transition metals, in the framework. By contrast, powder neutron diffraction offers the capacity to locate lithium in the presence of heavy-metal atoms,

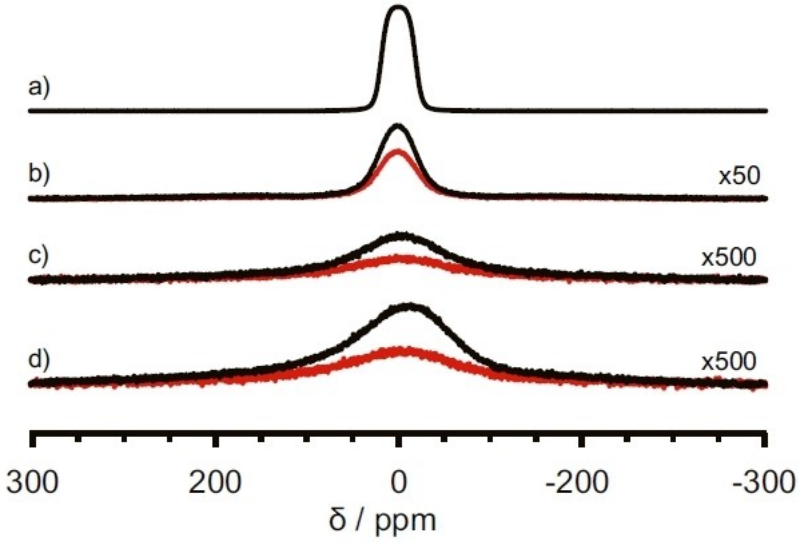

Figure 2. (a) The static ^{7}Li NMR spectrum of the reference compound LiCl. (b-d) Comparison of the NMR spectra recorded for investigated compounds with different levels of Li contents: 0.25 (black), 0.1 (red). (b) $CoSb_3$; (c) $Co_{0.5}Fe_{0.25}Ni_{0.25}Sb_3$; (d) $Fe_{0.5}Ni_{0.5}Sb_3$.

Table 2. A comparison of the ratio of the intensity of peaks in ^{7}Li NMR spectra of $Li_yCo_{1-2x}Fe_xNi_xSb_3$ with nominal lithium contents of 0.25 and 0.1, with the ratio of lithium contents determined experimentally by ICP-MS.

x in $Li_yCo_{1-2x}Fe_xNi_xSb_3$	Peak intensity ratio "$I_{0.25}/I_{0.1}$" determined by ^{7}Li-NMR	Ratio of lithium content y(0.25)/y(0.1) determined by ICP-MAS
0	1.44	1.14
0.125	1.50	1.23
0.25	1.90	1.97
0.375	5.19	2.11
0.5	4.24	2.85

owing to the greater relative magnitude of its coherent scattering length (b = −1.9 fm), while the appreciable difference from those of the framework atoms (Fe = 9.45 fm, Co = 2.49 fm and Ni = 10.3 fm, Sb = 5.57 fm)[43] also provides excellent contrast between the transition metals and antimony, enabling a detailed structural description to be obtained.

Whilst rare-earth[44] and alkaline-earth metal[45] fillers are located at the centre of transition-metal cubelets (*2a* site in *Im-3*), the smaller (r = 76 pm) Li^+ ion is potentially able to occupy alternative sites; including those located towards the centre of the Sb_4 rings (Figure 1b). Initial Rietveld refinement for $Li_yCo_{1-x}Fe_xNi_xSb_3$ was performed using only the framework atoms in the model, in order to generate a difference Fourier map ($|F_{obs}| - |F_{calc}|$) to identify possible locations for the intercalated lithium ions. Figure 3 presents, as an example, the 2-dimensional difference Fourier map for $Li_{0.25}Co_{0.5}Fe_{0.25}Ni_{0.25}Sb_3$. This exhibits negative peaks at the *2a* Wyckoff position, corresponding to the typical position for fillers in skutterudites, consistent with the negative coherent neutron scattering length of lithium. Significantly, there is no indication of the presence of lithium inside the planar rectangular four-membered Sb_4 rings, shown as orange rectangles in the 3D representations in Figure 3. We also explored the possibility that lithium is delocalised within the skutterudite cavity by allowing lithium cations to move off the 2*a* site to 16*f* sites (*x*, *x*, *x*). While the x-coordinate refined to values slightly less 0.5 (*x* = 0.42–0.46), this did not produce any significant improvement in the quality of the refinement. However, given the weak nature of the scattering from lithium, the possibility of a degree of delocalization of lithium ions within the cavity cannot be excluded completely.

Figure 4 presents the final Rietveld fits to the neutron diffraction patterns for $Li_yCo_{1-2x}Fe_xNi_xSb_3$ (y = 0.1 and 0.25, x = 0, 0.25, 0.5), from the Polaris 2θ~90° detector bank. The goodness-of-fit parameter, χ^2, reduces slightly on the introduction of lithium, with the maximum change (*ca.* 10% in the value of χ^2) observed for the most lithium-rich phase, $Li_{0.25}Fe_{0.5}Ni_{0.5}Sb_3$. Profiles from all Rietveld refinements using both the 90° and backscattering detector banks are provided as Supplementary Information (Figure S3). The final atomic coordinates, unit-cell parameters, and goodness of fit parameters are summarised in Table 3. The unit-cell parameter, *a*, increases with increasing levels of framework substitution (Figure 5), while at a given framework composition, the unit-cell parameter of lithiated phases is larger than that of the parent material, although it is relatively independent of lithium content, reflecting the small volume of a lithium cation, relative to the volume of the cavity. Refinement of the transition-metal and antimony site-occupancy factors did not result in any significant deviation from their nominal values or substantially improve the fit. Hence they were subsequently set to their nominal values. The site-occupancy factor of the lithium site was set to a value commensurate with the lithium content determined by ICP-MS. Attempts to refine the lithium atomic displacement parameter were unsuccessful and unrealistic values were obtained; the value was therefore constrained to $U_{iso} = 0.05$, an accepted value

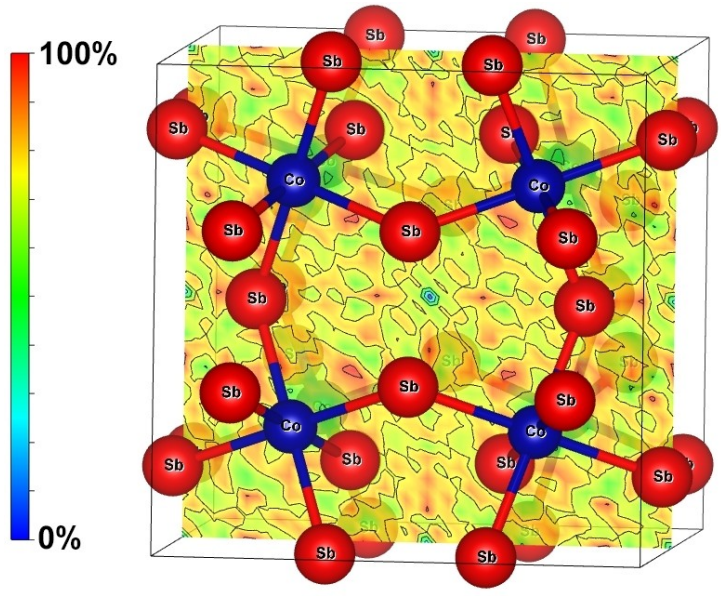

Figure 3. 2D difference Fourier map of $Li_{0.25}Co_{0.5}Fe_{0.25}Ni_{0.25}Sb_3$ in the (200) plane. Framework atoms are shown. The saturation colour scale shows the regions with negative (blue, 0% saturation) and positive scattering density (red, 100% saturation).

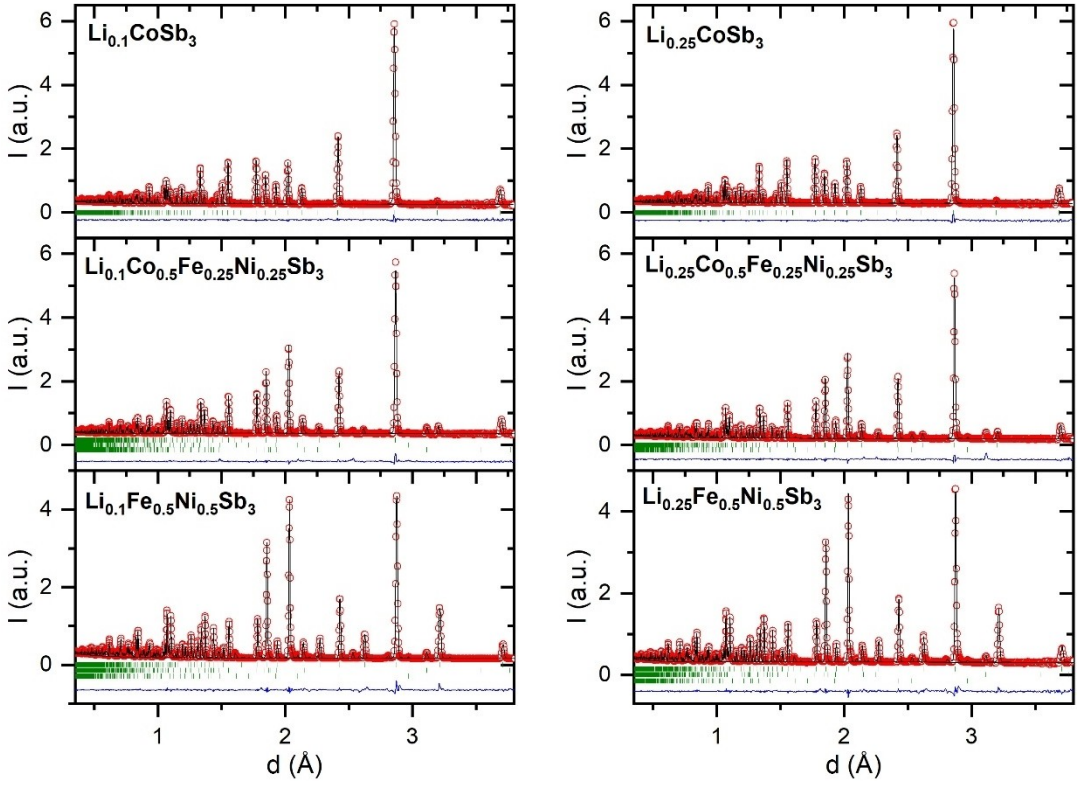

Figure 4. Fitted powder neutron diffraction patterns collected in the Polaris 2θ~90° detector bank for $Li_yCo_{1-2x}Fe_xNi_xSb_3$. Red circles are experimental observed data points, the black line is the calculated profile and the blue line is the difference profile (obs-calc). Vertical markers indicate the position of Bragg peaks (skutterudite phase, top; and where present Sb, middle; Fe_3O_4, bottom).

for a lithium atom vibrating in a structural cavity. A cylindrical absorption correction was applied during the refinements. Trace amounts of secondary phases Sb (< 3%) and Fe_3O_4 (< 0.7%) were detected in the data from materials containing Fe and Ni.

Table 3. Refined atomic parameters, from Rietveld analysis of powder neutron diffraction data collected from $Li_yCo_{1-2x}Fe_xNi_xSb_3$ ($y > 0.0$; $0.0 \leq x \leq 0.5$) at room temperature.[a]

x	**0.0**		**0.25**		**0.50**	
y	**0.1**	**0.25**	**0.1**	**0.25**	**0.1**	**0.25**
a/Å	9.03198(2)	9.03125(2)	9.05886(2)	9.05926(2)	9.08547(2)	9.08541(2)
y(Sb)	0.33500(3)	0.33495(3)	0.335033(5)	0.33513(4)	0.33527(6)	0.33519(6)
z(Sb)	0.15768(3)	0.15770(3)	0.157589(5)	0.15752(4)	0.15721(6)	0.15722(6)
U_{iso}(Sb)/Å^2	0.00524(2)	0.00518(2)	0.00550(5)	0.00555(4)	0.00634(7)	0.00623(5)
SOF(Sb)	1.0	1.0	1.0	1.0	1.0	1.0
U_{iso}(Fe.Co.Ni(/Å^2	0.00403(7)	0.00379(8)	0.00480(5)	0.00480(5)	0.00481(6)	0.00474(4)
SOF(Fe.Ni)	0.0	0.0	0.25	0.25	0.5	0.5
SOF(Co)	1.0	1.0	0.5	0.5	0.0	0.0
U_{iso}(Li)	0.05	0.05	0.05	0.05	0.05	0.05
SOF(Li)	0.065	0.075	0.05	0.105	0.05	0.145
Wt% Fe_3O_4	–	–	0.2(1)	0.58(7)	0.7(2)	0.8(3)
Wt% Sb	–	–	3.6(2)	–	3.3(2)	3.3(2)
Wt% $FeSb_2$	–	–	–	–	4.6(2)	3.3(1)
$R_{wp}(R_p)$/%						
$2\theta = 146°$	1.55(2.19)	1.77(2.50)	2.09 (2.60)	2.18 (3.08)	2.83(3.75)	2.10 (2.83)
$2\theta = 90°$	1.43(2.35)	1.45(2.38)	1.99 (2.59)	2.07 (3.44)	2.81(3.71)	2.08(2.85)
χ^2	1.92	1.97	4.89	3.87	6.52	4.79

[a] Space group: $Im\bar{3}$. Co/Ni/Fe on 8*c* ($^1/_4$ $^1/_4$ $^1/_4$); Sb on 24 *g* (0, *y*, *z*); Li on 2*a* (0, 0, 0).

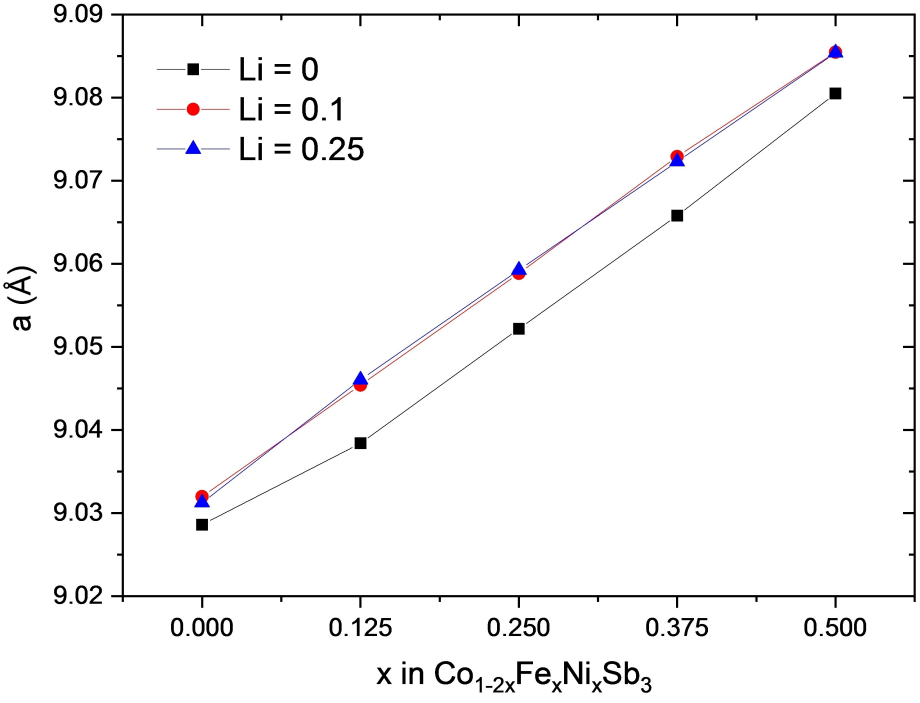

Figure 5. Variation of the unit-cell parameter with the level of framework substitution (x) for unfilled ($y = 0$, black squares) and lithiated ($y = 0.1$, red circles; $y = 0.25$ blue triangles), skutterudites, $Li_yCo_{1-2x}Fe_xNi_xSb_3$. Error bars lie within the points.

The electrical resistivity decreases significantly on lithiation and $\rho(T)$ becomes more metal-like with increasing lithium content (Figure 6a). This is due to an increase in charge carrier concentration, arising from electron transfer from the intercalated lithium guest to the framework. A similar result has previously been reported for Li_xCoSb_3 samples prepared by high pressure synthesis,[19] where the decrease of the resistivity with increasing temperature in the lithiated samples is attributed to a combination of charge carriers donated by intercalated lithium and of thermally activated carriers at higher temperatures. The $\rho(T)$ behaviour of $Li_yCo_{0.5}Fe_{0.25}Ni_{0.25}Sb_3$ and $Li_yFe_{0.5}Ni_{0.5}Sb_3$ ($y = 0.1$ and 0.25) shown as an inset to Figure 6a reveals that the lowest resistivity is exhibited by the material with the highest lithium content, which as noted above also requires the framework to contain the lowest levels of cobalt ($x = 0.5$). The increase in metallic-like character leads to a

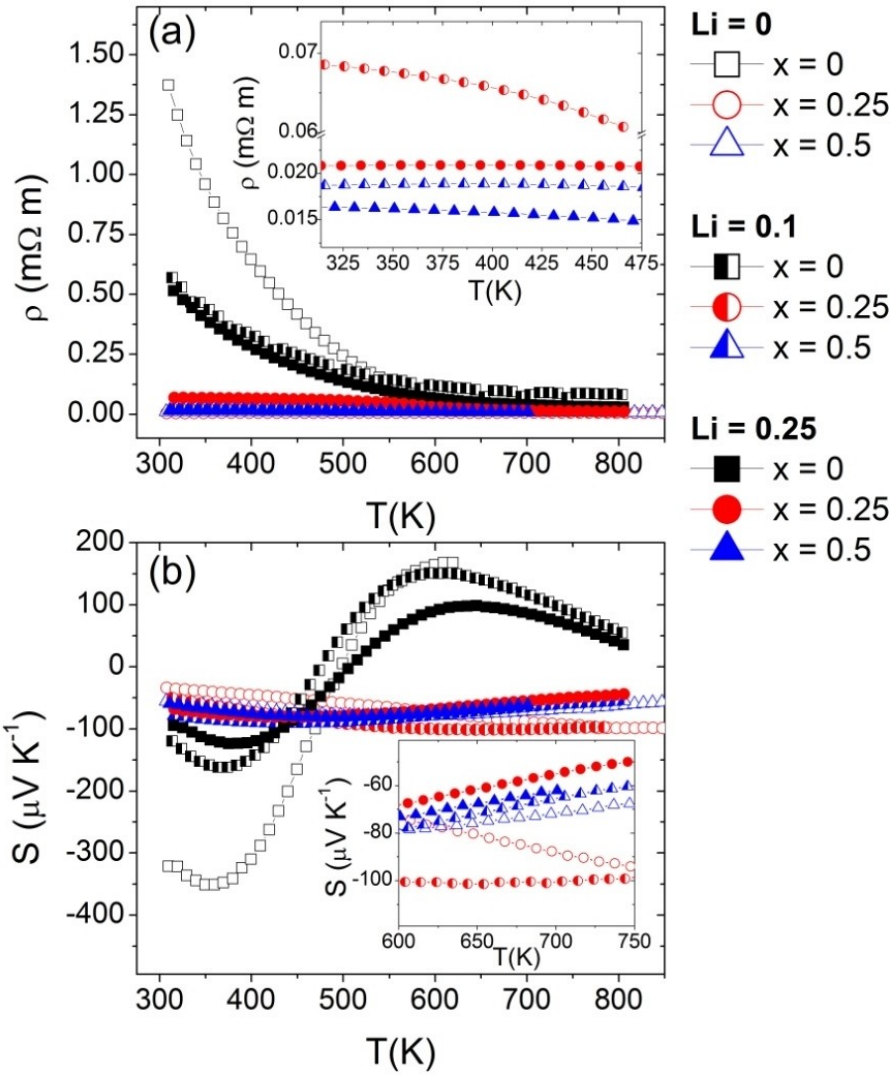

Figure 6. a) Temperature dependence of the electrical resistivity for unfilled and lithium-filled skutterudites. The inset is a magnification of the y-axis, where the decrease in resistivity with an increase in lithium filling for $Li_yCo_{0.5}Fe_{0.25}Ni_{0.25}Sb_3$ and $Li_yFe_{0.5}Ni_{0.5}Sb_3$ samples is more clearly observed. b) Temperature dependence of the Seebeck coefficient for the same samples. The inset shows *S*(T) for unfilled and lithiated $Co_{0.5}Fe_{0.25}Ni_{0.25}Sb_3$ and $Fe_{0.5}Ni_{0.5}Sb_3$ samples in more detail.

reduction in the absolute value of the Seebeck coefficient (Figure 6b). This effect is clearly observed for Li_yCoSb_3 samples where the magnitude of the Seebeck coefficient decreases from $-336\ \mu V K^{-1}$ in $CoSb_3$ to $-120\ \mu V K^{-1}$ and $-93\ \mu V K^{-1}$ in $Li_{0.1}CoSb_3$ and $Li_{0.25}CoSb_3$, respectively. In the case of $Li_yCo_{0.5}Fe_{0.25}Ni_{0.25}Sb_3$ and $Li_yFe_{0.5}Ni_{0.5}Sb_3$ (y = 0, 0.1 and 0.25) the change in Seebeck coefficient is less marked, especially in the case of $Li_{0.1}Co_{0.5}Fe_{0.5}Ni_{0.5}Sb_3$, for which the magnitude of the Seebeck coefficient is slightly higher than that for $Co_{0.5}Fe_{0.5}Ni_{0.5}Sb_3$ (inset Figure 6b). These variations in Seebeck coefficient and electrical resistivity affect the power factor ($S^2\sigma$), the temperature dependence of which is provided as Supplementary Information (Figure S4).

The presence of lithium in the cavities of the skutterudite framework leads to a reduction in thermal conductivity (Figure 7) from that of the unfilled skutterudites. This may be associated with resonant phonon scattering arising from localised vibrational modes of the Li^+ cations within the voids, which has been shown to cause a reduction in the thermal conductivity from that of the host lattice.[12,28] Comparing the thermal conductivity for the unfilled parent skutterudite with that for the two different levels of lithium incorporation (Figure 7), reveals a reduction in thermal conductivity of *ca.* 14% for $CoSb_3$ on lithiation. A significantly greater reduction in thermal conductivity is observed for substituted frameworks, reaching *ca.* 47% and 36%, for $Li_yCo_{0.5}Fe_{0.25}Ni_{0.25}Sb_3$ and $Li_yFe_{0.5}Ni_{0.5}Sb_3$ respectively. The lattice thermal conductivity (κ_L), estimated by subtracting the electronic component from the total thermal conductivity, is also presented in Figure 7. The reduction is similar for Fe and Ni containing samples (*ca.* 30%), suggesting that the electronic contribution (κ_e) is more significant, owing to the charge donation from the lithium

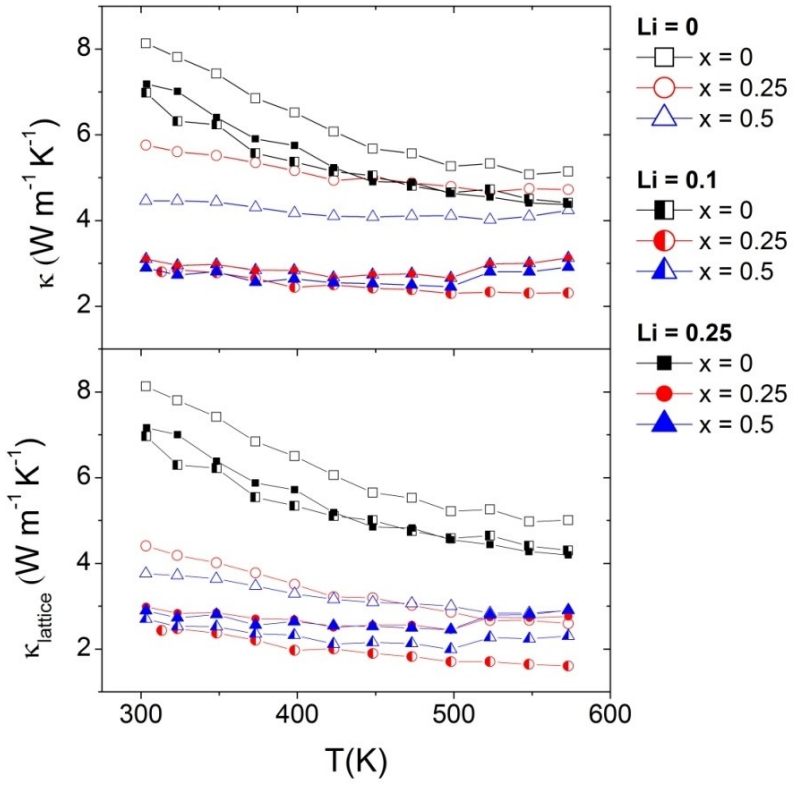

Figure 7. Temperature dependence of the: total thermal conductivity (top) and lattice thermal conductivity (bottom) for unfilled and lithium-filled skutterudites.

guest to the framework, while in the case of Li_yCoSb_3 the reduction in lattice thermal conductivity is similar to that for the total thermal conductivity value, indicating that the latter is dominated by the lattice contribution. This reduction in κ is sufficient to produce a slight enhancement in the figure of merit *ZT* at some compositions, with the maximum of $ZT = 0.12$ being obtained for $Li_{0.1}Co_{0.5}Fe_{0.25}Ni_{0.25}Sb_3$ at 573 K (Figure S5). This suggests that to optimise the thermoelectric response and obtain competitive values of the figure of merit suitable for applications, it is necessary to tune the electron count of the framework and compensate for charge transfer from the lithium guest. Relaxing the constraint of $a = b$ in the framework formula $Co_{1-a-b}Fe_aNi_bSb_3$ such that $a > b$, would provide one mechanism for compensating the additional charge transferred to the framework on intercalation of Li^+.

Conclusions

The introduction of lithium into the cavities of skutterudites of general formula $Co_{1-|x}Fe_xNi_xSb_3$ ($0 \leq x \leq 0.5$) was accomplished by an intercalation process at the modest temperature of 60 °C, affording a milder and less energy-intensive process than the conditions of high temperature and pressure previously reported for lithium-filling of skutterudites. ICP-MS and ^7Li solid state NMR data confirm the presence of lithium in intercalated phases, while Rietveld analysis of powder neutron diffraction data, in conjunction with difference Fourier synthesis, locate the intercalated lithium cations within the cavities of the skutterudite framework. Significant reductions in the thermal conductivity are observed as a result of intercalation of lithium cations, indicative of PGEC-type behaviour. However, the charge-transfer from the lithium ion to the framework that accompanies intercalation also impacts on the electrical-transport properties. In particular, materials become more metallic, exhibiting lower resistivities and, significantly, reduced Seebeck coefficients. This limits the figures of merit to relatively modest values, despite the reduced thermal conductivity and suggests a wider ranging investigation is required to optimize the charge-carrier concentration through control over the degree of intercalation and the framework composition, which has been shown to impose a limit on the maximum degree of lithium uptake, in order to enhance thermoelectric properties.

Acknowledgements

The authors wish to thank the UK Engineering and Physical Sciences Council (EP/K019767/1) for financial support and The University of Reading for access to the Chemical Analysis Facility. Neutron scattering beamtime (RB1610253) at the ISIS neutron and muon source was provided by the UK Science and Technology Facilities Council (STFC). The authors would like to

thank Johnson Matthey (JM Technology Centre, Sonning Common, UK) for carrying out ICP measurements.

Conflict of Interest

The authors declare no conflict of interest.

Data Availability Statement

The data that support the findings of this study are openly available in ISIS Neutron and Muon Source Data Journal at https://doi.org/10.5286/ISIS.E.RB1610253, reference number 1610253.

[1] R. Freer, A. V. Powell, *J. Mater. Chem. C* **2020**, *8*, 441–463.
[2] H. J. Goldsmid, *Introduction to thermoelectricity* Springer: **2010**, Vol. 2, p 278.
[3] G. J. Snyder, E. S. Toberer, *Nat. Mater.* **2008**, *7 (2)*, 105–114.
[4] A. Majumdar, *Science* **2004**, *303 (5659)*, 777–778.
[5] G. S. Nolas, J. Sharp, J. Goldsmid, *Thermoelectrics: basic principles and new materials developments* Springer Science & Business Media: **2013**; Vol. 45.
[6] T. M. Tritt, M. Subramanian, *MRS Bull.* **2006**, *31 (03)*, 188–198.
[7] G. A. Slack, *CRC Handbook of Thermoelectrics*, edited by D. M. Rowe (CRC Press, Boca Raton, FL, **1995**), Chap. 34, p. 407.
[8] Z. H. Ge, W. J. Li, J. Feng, F. Zheng, C. L. Jia, D. Wu, L. Jin, *Adv. Energy Mater.* **2022**, *12*(15), 2103770.
[9] M. Rull-Bravo, A. Moure, J. F. Fernandez, M. Martin-Gonzalez *RSC Adv.* **2015**, *5*, 41653.
[10] F. J. DiSalvo, *Science* **1999**, *285*, 703.
[11] B. Sales, D. Mandrus, R. K. Williams, *Science* **1996**, *272*, 1325.
[12] G. Nolas, D. Morelli, T. M. Tritt, *Annu. Rev. Mater. Sci.* **1999**, *29*, 89.
[13] J. Prado-Gonjal, P. Vaqueiro, C. Nuttall, R. Potter, A. V. Powell, *J. Alloys Compd.* **2017**, *695*, 3598.
[14] J.-W. Bos, *Intermetallic Thermoelectrics – Design, and Preparation of Half-Heulsers, Skutterudites and Zintl-type Materials, Inorganic Thermoelectric Materials* edited by A. V. Powell (Royal Society of Chemistry, Cambridge, **2022**), Chap. 5, p. 216–283.
[15] G. Rogl, P. F. Rogl, *Crystals* **2022**, *12*, 1843.
[16] I. Oftedal, *Norsk, Geol. Tidssk* **1928**, *8*, 250.
[17] F. Bridges, *Mod. Phys. Lett. B* **2016**, *30*, 163000.
[18] Y. Z. Pei, J. Yang, L. D. Chen, W. Zhang, J. R. Salvador, J. Yang, *Appl. Phys. Lett.* **2009**, *95*, 042101.
[19] G. Meisner, D. Morelli, S. Hu, J. Yang, C. Uher, *Phys. Rev. Lett.* **1998**, *80*, 3551.
[20] J. Yang, D. Morelli, G. Meisner, W. Chen, J. Dyck, C. Uher, *Phys. Rev. B* **2003**, *67*, 165207.
[21] Z. Y. Liu, J. L. Zhu, X. Tong, S. Niu, W. Y. Zhao, *J. Adv. Ceram.* **2020**, *9*, 647–673.
[22] X. Shi, H. Kong, C.-P. Li, C. Uher, J. Yang, J. R. Salvador, H. Wang, L. Chen, W. Zhang, *Appl. Phys. Lett.* **2008**, *92*, 182101.
[23] X. Tang, H. LI, Q. Zhang, M. Niino, T. Goto, *J. Appl. Phys.* **2006**, *100*, 123702.
[24] R. Liu, J. Yang, X. Chen, X. Shi, L. Chen, C. Uher, *Intermetallics* **2011**, *19*, 1747.
[25] X. Tong, Z. Liu, J. Zhu, T. Yang, Y. Wang, A. Xiai, *Front. Mater.* **2021**, *15*, 317.
[26] G. Rogl, A. Grytsiv, P. Rogl, E. Bauer, M. A. Zehetbauer, *Intermetallics* **2011**, *19*, 546.
[27] Y. Z. Pei, L. D. Chen, W. Zhang, X. Shi, S. Q. Bai, X. Y. Zhao, Z. G. Mei, X. Y. Li, *Appl. Phys. Lett.* **2006**, *89*, 221107.
[28] J. Zhang, B. Xu, L.-M. Wang, D. Yu, Z. Liu, J. He, Y. Tian, *Appl. Phys. Lett.* **2011**, *98*, 072109.
[29] J. Gainza, F. Serrano-Sánchez, J. E. Rodrigues, J. Prado-Gonjal, N. M. Nemes, N. Biskup, O. J. Dura, J. L. Martinez, F. Fauth, J. A. Alonso, *Adv. Funct. Mater.* **2020**, *30*, 2001651.
[30] J. Zhang, B. Xu, L.-M. Wang, D. Yu, J. Yang, F. Yu, Z. Liu, J. He, B. Wen, Y. Tian, *Acta Mater.* **2012**, *60*, 1246.
[31] J.-M. Tarascon, M. Morcrette, L. Dupont, Y. Chabre, C. Payen, D. Larcher, *J. Electrochem. Soc.* **2003**, *150*, A732.
[32] L. Zhang, X. Zhao, D. Xia, *Mater. Lett.* **2005**, *59*, 3448.
[33] L. Monconduit, J. Jumas, R. Alcantara, J. Tirado, C. P. Vicente, *J. Power Sources* **2002**, *107*, 74.
[34] A. V. Powell, *Light Atom Location in Filled Skutterudites*, STFC ISIS Neutron and Muon Source, **2015**, https://doi.org/10.5286/ISIS.E.RB1610253.
[35] R. I. Smith, S. Hull, M. G. Tucker, H. Y. Playford, D. J. McPhail, S. P. Waller, S. T. Norberg, *Rev. Sci. Instrum.* **2019**, *90*, 115101.
[36] A. C. Larson, R. B. Von Dreele, GSAS. GSAS, General Structure Analysis System. LANSCE, MS–H805, Los Alamos, New Mexico **1994**.
[37] K. Momma, F. Izumi, *J. Appl. Crystallogr.* **2008**, *41*, 653.
[38] R. D. Cowan, *J. Appl. Phys.* **1963**, *34*, 926.
[39] A. M. Chippindale, P. G. Dickens, A. V. Powell, *Progr. Solid State Chem.* **1991**, *21*, 133.
[40] J–P. Fleurial, T. Caillat, *Borshchevsky, Proc. ICT97, 16th Int. Conf. on* Thermoelectrics, Dresden, Germany, **1997**, IEEE, Cat. No.97TH8291.
[41] V. I. Bakhmutov, *Chem. Rev.* **2010**, *111*, 530.
[42] M. Kaupp, F. H. Köhler, *Coord. Chem. Rev.* **2009**, *253*, 2376.
[43] V. F. Sears, *Neutron News* **1992**, *3*, 26.
[44] Y. Dong, P. Puneet, T. M. Tritt, G. S. Nolas, *J. Soild State Chem.* **2014**, *209*, 1.
[45] L. Chen, X. Tang, T. Goto, T. Hirai, *J. Mater. Res.* **2000**, *15*, 2276.

Manuscript received: April 28, 2023
Revised manuscript received: June 30, 2023
Accepted manuscript online: July 17, 2023

